

# Synchrotron radiation induced magnetization in magnetically-doped and pristine topological insulators

A. M. Shikin<sup>1</sup>, D. M. Sostina<sup>1</sup>, A. A. Rybkina<sup>1</sup>, V. Yu. Voroshnin<sup>1</sup>, I. I. Klimovskikh<sup>1</sup>, A. G. Rybkin<sup>1</sup>, D. A. Estyunin<sup>1</sup>, K. A. Kokh<sup>1,2,3</sup>, O. E. Tereshchenko<sup>1,2,4</sup>, L. Petaccia<sup>5</sup>, G. Di Santo<sup>5</sup>, P. N. Skirdkov<sup>6,7,8</sup>, K. A. Zvezdin<sup>6,7,8</sup>, A. K. Zvezdin<sup>6,7,8</sup>, A. Kimura<sup>9</sup>, E. V. Chulkov<sup>1,10,11,12</sup>, and E. E. Krasovskii<sup>10,11,13</sup>

<sup>1</sup>Saint Petersburg State University, Saint Petersburg, 198504 Russia

<sup>2</sup>Novosibirsk State University, Novosibirsk, 630090 Russia

<sup>3</sup>V.S. Sobolev Institute of Geology and Mineralogy, Novosibirsk, 630090 Russia

<sup>4</sup>A.V. Rzhaznov Institute of Semiconductor Physics, Novosibirsk, 630090 Russia

<sup>5</sup>Elettra Sincrotrone Trieste, Strada Statale 14 km 163.5, 34149 Trieste, Italy

<sup>6</sup>Moscow Institute of Physics and Technology, Institutskiy per. 9, 141700 Dolgoprudny, Russia

<sup>7</sup>A.M. Prokhorov General Physics Institute, Russian Academy of Sciences, Vavilova 38, 119991 Moscow, Russia

<sup>8</sup>Russian Quantum Center, Novaya St. 100, 143025 Skolkovo, Moscow Region, Russia

<sup>9</sup>Graduate School of Science, Hiroshima University, 1-3-1 Kagamiyama, Higashi-Hiroshima 739-8526, Japan

<sup>10</sup>Departamento de Física de Materiales, Facultad de Ciencias Químicas, UPV/EHU, San Sebastián/Donostia, 20080 Basque Country, Spain

<sup>11</sup>Donostia International Physics Center (DIPC), San Sebastián/Donostia, 20018 Basque Country, Spain

<sup>12</sup>Centro de Física de Materiales CFM - MPC and Centro Mixto CSIC-UPV/EHU, San Sebastián/Donostia, 20080 Basque Country, Spain

<sup>13</sup>IKERBASQUE, Basque Foundation for Science, 48013 Bilbao, Spain

March 12, 2022

## Abstract

Quantum mechanics postulates that any measurement influences the state of the investigated system. Here, by means of angle-, spin-, and time-resolved photoemission experiments and ab initio calculations we demonstrate how non-equal depopulation of the Dirac cone (DC) states with opposite momenta in V-doped and pristine topological insulators (TIs) created by a photoexcitation by linearly polarized synchrotron radiation (SR) is followed by the hole-generated uncompensated spin accumulation and the SR-induced magnetization via the spin-torque effect. We show that the photoexcitation of the DC is asymmetric, that it varies with the photon energy, and that it practically does not change during the relaxation. We find a relation between the photoexcitation asymmetry, the generated spin accumulation and the induced spin polarization of the DC and V *3d* states. Experimentally the SR-generated in-plane and out-of-plane magnetization is confirmed by the  $k_{\parallel}$ -shift of the DC position and by the splitting of the states at the Dirac point even above the Curie temperature. Theoretical predictions and estimations of the measurable physical quantities substantiate the experimental results.

The photoexcitation by laser or synchrotron radiation is accompanied by a depopulation of the initial states, which influences the electronic structure observed in photoemission (PE) measurements. In materials with helical spin structure (for instance, topological insulators (TIs) [1, 2, 3, 4]) the imbalance in photoexcitation of the DC states with opposite momenta created, for instance, by circularly polarized laser or SR can be effectively used for the generation of the surface spin-polarized currents that depend on

the helicity of the radiation polarization [5, 6, 7, 8, 9, 10]. Similar to the case of an electric field applied in the surface plane [11, 12, 13], this can induce a magnetization in ferromagnetic TIs [8, 14]. The induced magnetic moment opens a gap at the Dirac point (DP) due to Time Reversal Symmetry (TRS) breaking providing a platform for the realization of unique quantum phenomena such as quantized magneto-electric effect [15, 16, 17] and quantum anomalous Hall effect [18, 19, 20] at elevated temperatures under light excitation. Although, the possibility of induced (and controlled) magnetization by linearly polarized SR has not been studied yet, the generation of spin-polarized current was noted recently [7, 8, 9, 1]. The present work aims to investigate a possibility of such SR-induced in-plane and out-of-plane magnetization in FM-doped and pristine TIs by linearly polarized SR. We relate this phenomenon to an asymmetry in the depopulation of the DC states with opposite momenta, which leads to a hole-generated uncompensated spin accumulation. The possibility of a long-living electron-hole separation between the excited electrons and generated holes (related to a reduced electron-phonon interaction at the surface [21, 22]) is confirmed by a series of time-resolved laser experiments (see, for instance, [23, 21, 22, 24]). The holes generated at the topological surface states (TSSs) are compensated by a drift of electrons from the TSSs out of the beam spot via long-time two-dimensional relaxation process [21]. In the case of a different probability of the photoexcitation of electrons from the DC states with opposite momenta, the uncompensated spin accumulation and the zero-bias spin-polarized photocurrent occur, as in Refs. [8, 9, 14], which can lead to induced magnetization similar to the case discussed in Ref. [25] for the (Ga,Mn)As ferromagnetic semiconductor.

The issue of SR-generated spin accumulation is strongly related to the TSS spin texture and to the asymmetry of the photoexcitation of the TSSs with opposite spin orientation. In Refs. [26, 27], it was shown that a total spin texture of TSSs includes not only contributions of the  $p_z$ -orbitals, but also of the  $p_x$ - and  $p_y$ -orbitals related to the radial and tangential components in the spin-orbital texture, which significantly modifies the spin texture of the TSSs probed by photoemission. Total spin structure in PE spectra depends on the sum of all contributions determined by optical selection rules, quantum interference and SR incident angle [28, 29, 30]. Due to variation of  $k_z$  with photon energy all  $p_{x,y,z}$  components “oscillate” with different phases. The non-trivial character of TSS spin texture is confirmed by spin-resolved photoemission both via theoretical analysis [31, 28, 29, 32, 33, 27, 30] and via experimental measurements [27, 28, 29, 30] using different polarization of SR [31, 34, 28, 29] and manifests itself in significant modification of the spin polarization of photoelectrons with photon energy [31, 28, 29, 32]. The oblique incidence of SR breaks the symmetry of the angular distribution of the photocurrent, and the different photoemission intensity at  $k_{||}$  and  $-k_{||}$  [28, 27] can be a source of the SR-generated uncompensated spin accumulation and an induced magnetization. This problem is especially important for magnetically-doped TIs because the DP gap opening due to the TRS breaking, its value and origin (magnetization- or hybridization-derived) are being actively discussed, see, for instance, Ref. [35]. However, without a proper analysis of the influence of the non-equal depopulation of the TSSs on a possible induced magnetization during ARPES and SARPES measurements such questions cannot be answered.

In the present work we study the PE intensity asymmetry of the DC states and connect it with the SR-generated asymmetric  $k_{||}$ -distribution of the holes and the resulting spin accumulation leading a local induced magnetization via spin-torque effect. The first part of the work aims to clarify how the photoexcitation by a linearly polarized SR influences the DC states intensity distribution in the ARPES intensity maps and how it varies with photon energy. In the second part we analyze how the imbalance in the depopulation of the TSSs in V-doped TI and the corresponding SR-generated uncompensated spin accumulation result in an induced in-plane and out-of-plane polarization of TSSs and the V  $3d$ -ions. Then, the laser pump-probe experiment allows us to conclude that the imbalance in the depopulation of the TSSs is practically not changed during the relaxation, and the SR-induced magnetization can be estimated in rough approximation using the TSS intensity asymmetry in PE spectra.

## Asymmetry in the intensity of the DC states vs photon energy

In this work we study a series of pristine and V-doped TIs with fractional stoichiometry based on  $\text{Bi}_2\text{Te}_2\text{Se}$  with inclusion of different Sb-concentrations. They have a wide insulating energy gap with the DP inside the bulk gap [36, 37] and an enhanced surface contribution to the spin transport [38], which is important for spintronics applications.

Figures 1(a,b,c) show the photon energy dependence of the TSS ARPES energy-momentum intensity maps measured along the  $\overline{\Gamma K}$  direction of the surface Brillouin zone using linearly  $p$ -polarized SR for pristine and for magnetically-doped TIs with the following stoichiometries: (a)  $\text{Bi}_{1.37}\text{Sb}_{0.5}\text{Te}_{1.8}\text{Se}_{1.2}$ , (b)  $\text{Bi}_2\text{Te}_2\text{Se}$ , and (c)  $\text{Bi}_{1.37}\text{V}_{0.03}\text{Sb}_{0.6}\text{Te}_2\text{Se}$ . In Fig. 1(g), the ARPES dispersions measured along the

$\overline{\Gamma M}$  direction for  $\text{Bi}_{1.37}\text{Sb}_{0.5}\text{Te}_{1.8}\text{Se}_{1.2}$  are shown for comparison. The geometry of the experiments is schematically presented in Methods Fig. 8. For the presented experiments the Geometries **1** and **2** were used with the analyzer entrance slit orientation along and perpendicular to the SR incidence plane. For Geometry **1** two different photon incidence angles have been used:  $73^\circ$  (a) and  $50^\circ$  (b),(c) relative to the surface normal (with measurements along  $\overline{\Gamma K}$ ). The intensity maps for  $\text{Bi}_{1.5}\text{Sb}_{0.5}\text{Te}_{1.8}\text{Se}_{1.2}$  along  $\overline{\Gamma M}$ , for  $\text{Bi}_{1.4}\text{Sb}_{0.6}\text{Te}_2\text{Se}$  along  $\overline{\Gamma K}$  and for  $\text{Bi}_{1.37}\text{V}_{0.03}\text{Sb}_{0.6}\text{Te}_2\text{Se}$  along  $\overline{\Gamma M}$  are presented in Supplementary Figs. 1S, 2S and 3S, respectively, with different orientation of the SR incidence plane. For Geometry **2**, the incidence angles was  $45^\circ$  (g) with measurements along  $\overline{\Gamma M}$ , orthogonal to the SR incidence plane (oriented along  $\overline{\Gamma K}$ ). Below each ARPES intensity map the profiles of the TSS intensities are presented for the constant-energy cut of the upper DC at the binding energy corresponding to a high intensity of the TSSs, see white lines in the ARPES maps. In all the profiles the intensities at opposite  $k_{\parallel}$  points are different. At some photon energies the intensity at positive  $k_{\parallel}$  is larger than at negative  $k_{\parallel}$ , and at other photon energies the relation is opposite. Figs. 1(d),(e),(f) collect all data measured for different TIs and demonstrate the photon energy dependence of the asymmetry in the intensity of the opposite TSS branches. The TSS intensity asymmetries are characterized by the ratio

$$A = \frac{I(-k_{\parallel}) - I(k_{\parallel})}{I(-k_{\parallel}) + I(k_{\parallel})}, \quad (1)$$

measured at the energies marked by white horizontal lines. The asymmetry  $A$  oscillates with photon energy both for pristine and for V-doped TIs.

In order to explain the observed  $k_{\parallel}$ -distribution of the photocurrent and its variation with the photon energy we have calculated *ab initio* the energy-momentum distribution of the photoemission intensity from the DC of the stoichiometric compound  $\text{Bi}_2\text{Te}_2\text{Se}$ . The electronic structure of  $\text{Bi}_2\text{Te}_2\text{Se}$  [36] is quite similar to that of the crystals with the fractional stoichiometry studied here. We use the one-step theory of photoemission in the dipole approximation, so the photocurrent from the state  $|\mathbf{k}_{\parallel}\rangle$  is proportional to the transition probability  $|\langle \Phi | -i\nabla_{\mathbf{e}} | \mathbf{k}_{\parallel} \rangle|^2$  to the time-reversed low energy electron diffraction state  $|\Phi\rangle$  [39], where  $-i\nabla_{\mathbf{e}}$  is the momentum operator in the direction of the light polarization  $\mathbf{e}$ . The final state  $|\Phi\rangle$  is calculated for the scattering of electrons on a semi-infinite crystal as explained in Ref. [40]. The inelastic scattering is included by adding a spatially constant imaginary part  $V_i = 1$  eV to the crystal potential. The crystal potential was obtained within the local density approximation with the full-potential linear augmented plane wave method [41]. The initial states were calculated within a two-component relativistic formalism [42] for a slab composed of 7 quintuple layers. Figs. 2(a-c) show the  $k_{\parallel}$ -distribution of the calculated photoemission intensity from the DC of  $\text{Bi}_2\text{Te}_2\text{Se}$  for the opposite  $\overline{\Gamma K}$  directions and Figs. 2(d-f) for the opposite  $\overline{\Gamma M}$  directions. In both cases the  $p$ -polarized SR is incident along  $\overline{\Gamma K}$  (Geometry **1**). The  $k_{\parallel}$ -integrated intensities for  $\overline{\Gamma K}$  and  $\overline{\Gamma M}$  are shown in Fig. 2(g) and 2(h), respectively. The corresponding asymmetry index for the light incident along  $\mathbf{k}_{\parallel}$  is shown in Fig. 2(i) and for the light incident perpendicular to  $\mathbf{k}_{\parallel}$  (Geometry **2**) in Fig. 2(j).

Note that when the light is incident along  $\mathbf{k}_{\parallel}$  the difference between  $+k_{\parallel}$  and  $-k_{\parallel}$  is due to a linear dichroism, and it strongly depends on the angle of incidence, see Fig. 2(i). In particular, along  $\overline{\Gamma K}$  the opposite directions are equivalent owing to the  $C_{3v}$  symmetry of the surface, and it is the light that breaks the symmetry of the experiment. On the contrary, for the light incident perpendicular to  $\mathbf{k}_{\parallel}$ , Fig. 2(j), the intensity asymmetry is due to the inequivalence of  $+k_{\parallel}$  and  $-k_{\parallel}$  along  $\overline{\Gamma M}$ . In that case the photon energy dependences  $I_{\text{left}}(h\nu)$  and  $I_{\text{right}}(h\nu)$  are very similar, see Fig. 2(h), and the intensity asymmetry does not strongly depend on  $\theta$ , see Fig. 2(j). The theory explains the experimentally observed oscillations of the asymmetry index with the photon energy and relates them to energy variations of the final state  $|\Phi\rangle$ .

## Hole generation analysis and asymmetry variation during relaxation

Let us assume that at the used SR energies the excited spin-polarized photoelectrons escape to a considerable degree into the vacuum. Then, the uncompensated spin accumulation generated by the different photoexcitation rate of electrons with opposite momenta and its orientation are mainly determined by the asymmetry in the concentration of the photo-holes in the opposite TSS branches. How to determine this asymmetry? In the simplest approximation one can infer the photo-hole concentration asymmetry and the related uncompensated spin accumulation from the asymmetry of the photocurrent from the DC states.

The second question is whether the asymmetry in the concentration of the photo-holes is preserved during the relaxation process. To clarify this we carried out a time-resolved pump-probe laser experiment, as in Refs. [23, 21, 22, 24]. The modification of the TSS intensity asymmetry measured for  $\text{Bi}_{1.97}\text{V}_{0.03}\text{Te}_{2.4}\text{Se}_{0.6}$  immediately after the photoexcitation (just under the laser pump pulse generation) and during the relaxation of photoexcited electrons is presented in Fig. 3(a). The scheme and geometry of the experiment [21, 24] are presented in Supplementary Fig. 4S. The probe pulse of  $h\nu = 5.9$  eV was linearly  $p$ -polarized. The pump pulse was  $s$ -polarized with  $h\nu=1.48$  eV. Below each ARPES map the intensity asymmetry profiles of the opposite DC branches are shown. These asymmetries were measured at an energy near the bottom of the conduction band (CB) marked by the horizontal dashed lines. These data show the time evolution of the intensity distribution of both the photoexcited electrons (above the Fermi level) and the de-occupied DC states (below the Fermi level). The variation of the depletion of the TSS intensity below the Fermi level can be an indicator of the hole generation and relaxation. One can see that the TSS intensity asymmetry observed at the moment of the electron photoexcitation is practically not changed during relaxation. The unchanged with time TSS asymmetry is observed also for other energy cuts, see Supplementary Fig. 5S. It allows us to make a very important qualitative conclusion that within this approximation the photo-hole generated asymmetry is not significantly transient with time. In other words, the asymmetry in the measured PE intensity of the TSSs with opposite momenta can be used for a rough estimate of the induced uncompensated spin accumulation and the related magnetization, as we discuss in detail in the next section.

## Estimations of the in-plane and out-of-plane spin polarization (magnetization) induced in V-doped and pristine TI by linearly polarized SR

In the following we discuss the theoretical estimations of the magnetization induced by linear  $p$ -polarized SR due to the generated uncompensated spin accumulation. First of all let us consider the symmetry of the spin accumulation induced by linearly polarized SR. Taking into account that this effect is caused by photoexcitation, the spin density  $\vec{S}$  can be considered as quadratic by the field:

$$\vec{S} = B_{ikl} E_k E_l, \quad (2)$$

where  $B_{ikl}$  is a 3rd rank pseudotensor and  $E_{k,l}$  are the components of electric field. Following to Refs. [43, 44] the Bi-based compounds are referred to the space group  $D_{3d}^5(R\bar{3}m)$ . In the presence of a [111] surface, the symmetry of the considered four-component complex compound can be reduced to  $C_3$ , and therefore  $B_{ikl}$  is equal [45]:

$$B_{ikl} = \begin{pmatrix} B_{11} & -B_{11} & 0 & B_{14} & B_{15} & -B_{22} \\ -B_{22} & B_{22} & 0 & B_{15} & -B_{14} & -B_{11} \\ B_{31} & B_{31} & B_{33} & 0 & 0 & 0 \end{pmatrix}, \quad (3)$$

where  $B_{i\mu} = B_{ikl}$  ( $kl \leftrightarrow \mu = 1, \dots, 6$ ) are the coefficients determined by the material. Considering the SR radiation as  $\vec{E} = (E \cos \psi, 0, E \sin \psi)^T$ , from the Eq. 3 it immediately follows that SR can excite both the in-plane and out-of-plane uncompensated spin accumulation. Assuming that the linearly polarized SR can be decomposed on right and left circularly polarized SR, which of them can depopulate mostly one of the Dirac cone branches [14], the averaged uncompensated spin accumulation can be represented empirically as  $\delta S_{x,z} = \frac{\hbar}{2} \xi_{x,z} P \tau A$ , where  $P$  is the probability of the electron photoexcitation per unit time,  $\tau$  is the decoherence time of the spins and  $\xi_{x,z}$  is an empirical constant. It should be noted that  $P\tau$  is the steady-state concentration of the generated holes. In the simplest case of semiconductor optical orientation  $\xi_x^0 = \sin \psi$  and  $\xi_z^0 = \cos \psi$  [46]. For simplicity, we assume that  $\xi_{x,z} = \kappa_{x,z} \xi_{x,z}^0$ , where  $\kappa_{x,z} \approx 1$ . Assuming that the magnetization of electron sub-system induced by linearly polarized SR can be estimated as  $m_{x,z} = \mu_B \kappa_{x,z} \xi_{x,z}^0 P \tau A$ , where  $\mu_B$  is the Bohr magneton and  $A$  is the TSS photoexcitation asymmetry (see also [14]).

In the case of the V-impurity subsystem, below the Curie temperature ( $T < T_C$ ) the total energy can be represented as  $E_V = -K_U (m_z^V)^2 - (\vec{m}^V \cdot \vec{H}_{SR})$  where  $K_U$  is the constant of uniaxial anisotropy,  $m_z^V$  is the z-axis component of the V-subsystem magnetization,  $\vec{H}_{SR} = H_{SR} (\kappa_x \sin \psi, 0, \kappa_z \cos \psi)^T$  is the field acting on the V impurities from the SR induced magnetization,  $H_{SR} = \frac{\tilde{a}^2}{\mu_B} J_{eV} P \tau A$ , where  $\tilde{a} = 4.24 \text{ \AA}$  is the lattice constant typical of the studied TIs,  $J_{eV} \approx 0.3 \text{ eV}$  [47, 48, 49] is the exchange constant, which



describes the ( $s - d$ ) interaction between the TSSs and the V-ion impurities system. In case ( $T > T_C$ ) the energy minimization leads to the following expression for the V-subsystem magnetization:

$$\vec{m}^V = g\mu_B S N B_S (g\mu_B S H_{SR}/T) (\sin \eta, 0, \cos \eta)^T, \quad (4)$$

where  $g \approx 2$  is the g-factor,  $S = 3/2$  is the spin of impurity ion,  $N$  is the averaged impurity concentration,  $B_S$  is the Brillouin function and  $\eta$  is slightly differs from  $\psi$  and  $\sin \eta = \kappa_x \sin \psi / \sqrt{\kappa_x^2 \sin^2 \psi + \kappa_z^2 \cos^2 \psi}$ . In case of ( $T < T_C$ ) we also have to consider anisotropy, but estimations proves that the anisotropy term is significantly smaller than the SR term (see Supplementary Inform. for details), therefore, Eq. 4 is valid with a good accuracy for all temperature range. The dependence of the in-plane component of the total magnetization  $\vec{M} = \vec{m} + \vec{m}^V$  (under experimental conditions  $\psi = 50^\circ$  and  $P\tau \approx 3.5 \times 10^{13} \text{ cm}^{-2}$ ) on the in-plane asymmetry value ( $A$ ) for different temperatures is represented on Fig. 4(a).

The complete electron Hamiltonian of the considered system including both electron-electron and electron-vanadium interactions in the mean field approximation can be written as:

$$\hat{H}_e = \hbar V_D [\vec{k} \times \vec{\sigma}] \vec{e}_z + \frac{\tilde{a}^2}{\mu_B} J_{eV} (\vec{m}^V \cdot \vec{\sigma}) + \frac{\tilde{a}^2}{\mu_B} U (\vec{m} \cdot \vec{\sigma}), \quad (5)$$

where  $V_D \sim 5.3 \times 10^7 \text{ cm/s}$  is the velocity taken from the TSS dispersion law,  $\vec{\sigma}$  is the vector of Pauli matrices and  $U \approx 0.2 \text{ eV}$  is the Hubbard parameter. The energy spectrum in this case has the following form:

$$E = \pm \sqrt{\hbar^2 V_D^2 |\vec{k}|^2 + \Delta_x^2 + \Delta_z^2 - 2\hbar V_D k_y \Delta_x}, \quad (6)$$

where

$$\begin{aligned} \Delta_x &= \frac{\tilde{a}^2}{\mu_B} J_{eV} m_x^V + \frac{\tilde{a}^2}{\mu_B} U m_x \\ \Delta_z &= \frac{\tilde{a}^2}{\mu_B} J_{eV} m_z^V + \frac{\tilde{a}^2}{\mu_B} U m_z \end{aligned} \quad (7)$$

The resulting band structure modification under influence of the induced out-of-plane and in-plane magnetization is shown in Fig. 4(b) (under experimental conditions noted above and the averaged value of the asymmetry of  $A = 0.5$  taken from Fig. 5(a)). The out-of-plane magnetization is accompanied by the splitting of the DC states at the DP. The induced in-plane magnetization emerges in the  $k_{\parallel}$ -shift of the DC in the direction orthogonal to the induced magnetic field (or magnetization). (Analogous  $k_{\parallel}$ -shift is observed under external applied in-plane magnetic field [8, 50, 51]). Corresponding calculated temperature dependence of the DP-gap value and the  $k_{\parallel}$ -shift of the DP position in the direction orthogonal to the magnetization are presented in Figs. 4(c,d) (see the discussion below).

## Experimental confirmation of the induced in-plane magnetization

As an experimental evidence of the SR-induced in-plane magnetization, Fig. 5 demonstrates a correlation between the modification of the experimental intensity maps of the upper DC states close to the Fermi level (line 5(a)) and the  $(k_x, k_y)$ -shift of the DP position induced by the in-plane magnetic field generated by SR with linear  $p$ - and opposite circular polarizations (line 5(b)), which is expected in accordance with Fig. 4(b). The incident direction of SR corresponds to the vertical line. For each of the DC energy cuts (Fig. 5(a)) the TSS intensity profiles in the  $k_x, k_y$ -directions are presented, in the bottom and right graphs, respectively. These profiles clearly demonstrate a pronounced modulation of the intensity of the DC states intensity and their asymmetry both along and orthogonally to the SR incidence plane. The maps were measured with  $\hbar\nu = 28 \text{ eV}$  for  $\text{Bi}_{1.37}\text{V}_{0.03}\text{Sb}_{0.6}\text{Te}_2\text{Se}$  kept at the temperature of 55K. The DP positions (Fig. 5(b)) were estimated from the maximal intensity of the TSS in  $k_x$  and  $k_y$ , see the profiles at the bottom and on the right side of the maps cut at the DP. The different depopulation of the opposite DC states under photoexcitation with different polarization of SR is well visible in Fig. 5(a), and it leads to the  $(k_x, k_y)$ -shift of the DC according to the direction of induced magnetic field, which is determined by the asymmetry in the TSS intensity. The direction of the uncompensated spin accumulation and of the induced in-plane magnetic field are determined by the direction where the TSS intensity asymmetry is oriented and by the details of the spin texture [26, 27, 28]. The relation between the experimental TSS intensity asymmetry ( $A$ ), the direction of the induced magnetic field ( $M$ ) generated by uncompensated spin accumulation ( $S$ ) in correspondence to spin texture and direction of the DP position  $(k_x, k_y)$ -shift is schematically shown in Fig. 5(c). For circularly polarized SR a pronounced asymmetry in the TSS

intensity is observed in the direction perpendicular to the SR incidence. The use of the opposite circular polarizations leads to the TSS intensity asymmetry and generated uncompensated spin accumulation with spin orientation (and corresponding magnetic moment) in opposite  $k_{\parallel}$ -directions. This direction of the induced magnetic field determines the shift of the DP orthogonally to the SR incidence ( $k_x$ ) that is confirmed experimentally (see the shift of blue crosses in comparison with the green one). For linear  $p$ -polarization of SR the TSS intensity asymmetry is observed in the direction along the SR incidence. This leads to a spin accumulation (S) and magnetic field (M) perpendicular to the SR incidence. As a result, the  $k_y$ -shift of the DP position is observed in the direction orthogonal to that in the case of a circularly polarized SR. The measurements at room temperature (Supplementary Fig. 6S) and at 30K at the 9B beamline HiSOR (Hiroshima, Japan) albeit with a lower intensity of SR (not shown) demonstrate similar behavior. The value of the  $k_{\parallel}$ -shift of the Dirac cone induced by linearly-polarized SR shown in Fig. 5 (in comparison with the DC position under excitation by circularly polarized SR) can be estimated to approximately  $5 - 10 \times 10^{-3} \text{ \AA}^{-1}$  in agreement with the theoretical estimation of the  $k_{\parallel}$ -shift in Fig. 4(b). Lower value of the  $k_{\parallel}$ -shift of the DP position at room temperature presented in Supplementary Fig. 6S confirms the calculated temperature dependence of the DP  $k_{\parallel}$ -shift shown in Fig. 4(d). Under excitation by a circularly polarized SR of opposite chirality the  $k_{\parallel}$ -shift of the DC position is stronger, which is related to the enhanced TSS intensity asymmetry (see corresponding profiles).

Additionally, the in-plane magnetization induced by a linearly polarized SR can be confirmed by the  $k_{\parallel}$ -shift of the spin-polarized DC states relative to the non-spin-polarized CB states. (A similar  $k_{\parallel}$ -shift under applied magnetic field was noted in Ref. [8]). Supplementary Fig. 7S demonstrates that such  $k_{\parallel}$ -shift is actually observed at different photon energies, and it is important that the direction of the  $k_{\parallel}$ -shift is related to the observed TSS intensity asymmetry. It is interesting that the value of the  $k_{\parallel}$ -shift relative to  $k_{\parallel} = 0$  can be also estimated to be about  $10 \times 10^{-3} \text{ \AA}^{-1}$ , which correlates with the estimations noted above. Moreover, when the sign of the asymmetry changes with photon energy the DC shifts in the opposite direction. This confirms that the observed shift is really connected with the TSS intensity asymmetry and the resulting induced in-plane magnetization direction. The  $k_{\parallel}$ -shift of the DC branches relative the CB states located at  $k_{\parallel} = 0$  is also observed in the case of photoexcitation by laser radiation. In that case the profiles shown in Fig. 3(b) below the ARPES dispersion map (cut at the energy marked by white line which crosses both DC and CB states) demonstrate non-equal distance from the left and right side.

As a partial conclusion we have experimentally observed the DP position ( $k_x, k_y$ )-shifts in accord with the measured asymmetry of TSS intensity confirming that the non-equal depopulation of these states induces the in-plane magnetic fields under photoexcitation by SR.

## Out-of-plane induced magnetization and its experimental confirmation

Let us now discuss the problem of the out-of-plane magnetization induced by linearly polarized SR. Fig. 6(a) shows the calculated photon energy dependence of the out-of-plane net-spin photocurrent  $S(k_{\parallel}, h\nu) = I^{\uparrow}(k_{\parallel}, h\nu) - I^{\downarrow}(k_{\parallel}, h\nu)$  from the upper DC of  $\text{Bi}_2\text{Te}_2\text{Se}$  with the SR incident along  $\overline{\Gamma\text{K}}$ . The out-of-plane net-spin-photocurrent integrated over  $k_{\parallel}$  does not vanish, and its photon energy dependence is shown in Fig. 6(b). The magnitude and the sign of the integral photocurrent are seen to vary with the photon energy, which suggests that also the total out-of-plane spin accumulation may be different for different photon energies. This out-of-plane spin accumulation generates the induced out-of-plane magnetization that should lift the degeneracy of the TSSs and open the energy gap at the DP due to the TRS breaking, as in Refs. [14, 52] under circularly polarized SR. Using Eq. 7 one can estimate the energy gap as  $\Delta = 2 \frac{\tilde{a}^2}{\mu_B} J_{eV} m_z^V + 2 \frac{\tilde{a}^2}{\mu_B} U m_z$ .

Fig. 4(c) shows the calculated temperature dependence of the gap induced at the Dirac point using the value of the TSS asymmetry of 0.3 (as averaged value taken from the asymmetry values presented in Fig. 5(a) and Fig. 1(e) at  $h\nu = 28 - 30 \text{ eV}$ ) both for magnetically-doped and for pristine TIs at the experimental conditions noted above (see Methods for details).

For magnetically-doped TI below 30 K a gap of about 25 meV is expected. As temperature increases the gap decreases down to 12–15 meV at room temperature. A finite gap above the Curie temperature is just related to the out-of-plane magnetization generated by SR. In the case of pristine TI a formation of the gap of 4.5 meV is expected too, independently on temperature. Unfortunately the energy resolution in our conditions was not high enough to allow the measurement of this small gap value within a reasonable experimental error.

The experimentally measured in-plane and out-of-plane spin polarization is presented in spin-resolved spectra in Figs. 7(a,b). The spectra were measured for  $\text{Bi}_{1.31}\text{V}_{0.03}\text{Sb}_{0.66}\text{Te}_2\text{Se}$  at the temperature of 23 K

at the DP by using linear  $p$ -polarized SR. The corresponding experimental polarization asymmetry is plotted in the bottom part of the graphs. The spin orientation was measured along the SR incidence plane (Geometry 1). The related ARPES intensity map is shown in the inset in the upper central part. The spin-resolved spectrum in Fig. 7(a) confirms the in-plane spin-polarization of the states in the region of the DP, which is inverted relative to the DP (see black arrows on the polarization asymmetry). The observed in-plane polarization along the SR incidence plane is determined by the contribution of the  $p_x, p_y$  components in the spin texture. Similar effects are described in Refs. [53, 30]. The generated out-of-plane polarization is shown in Fig. 7(b). The presented spin-resolved spectrum demonstrates availability of the spin-polarized states at the Fermi level. We ascribe these states to the V  $3d$ -resonances characterized by the out-of-plane spin polarization. It is known that for V-doped TIs the maximal intensity of the V  $3d$ -ion states is located near the Fermi level [54, 20]. The magnetically-doped TIs are characterized by a colossal anisotropy of the magnetic moment induced at the FM-impurity atoms, which favors the magnetization perpendicular to the surface. Therefore, the observed out-of-plane spin polarization of the states near the Fermi level can signify the out-of-plane magnetization of the V  $3d$ -ions.

The SR-induced out-of-plane magnetization can be also experimentally confirmed by the splitting of the TSSs and opening of the energy gap at the DP both below and above the Curie temperature (see discussion above). Figs. 7(c,d) demonstrate the spin-integrated spectra measured directly at the DP for V-doped TIs at the temperatures of 1 K and 66 K, below and above the Curie temperature, respectively (which is below 5-10 K), in comparison with that measured for pristine TI at room temperature – Fig. 7(e). The relevant ARPES intensity maps are presented above each spectrum to show the DP positions. The fitting procedures for the spectra measured for V-doped TIs (Figs. 7(c,d)) show a decomposition into two spectral components with the energy splitting of about 20-25 meV at the DP below and above the Curie temperature. The width of the components was chosen in accord with the width of the TSS peaks outside the DP extracted from the ARPES intensity maps. The splitting into two components for the states at the DP above the Curie temperature (when a spontaneous magnetic order is destroyed) allows us to conclude that the out-of-plane magnetization is induced by SR. The spectra for other TIs presented in Supplementary Fig. 8S demonstrate similar behavior with the splitting of the TSSs at the DP. At the same time, the spectra measured at the DP for pristine TI (Fig. 7(e) and Supplementary Fig. 8S) do not show a noticeable splitting at the DP. The fitting procedure for these spectra shows only a one-component structure. The splitting of 4.5 meV predicted by theoretical estimations for pristine TI (Fig. 4(b)), is not resolved in our experiment. Thus, for TI without magnetic doping the photoexcitation by SR does not lead to a noticeable out-of-plane magnetization. Therefore, one can conclude that the splitting of the states at the DP in magnetically doped TIs can actually be an indicator of the induced out-of-plane magnetization generated by the linearly-polarized SR.

**In summary**, we have demonstrated that the asymmetry of the DC states with opposite spin orientation in photoexcitation by  $p$ -polarized SR is accompanied in pristine and magnetically-doped TIs by an uncompensated spin accumulation of the generated holes in the initial states. This leads to the in-plane and out-of-plane polarization of the TSSs and the V  $3d$ -ions and corresponding magnetization via the spin-torque effect. Experimentally it is indicated by spin-resolved PE spectra and is confirmed by the  $k_{\parallel}$ -shift of the DC position under the induced in-plane magnetic field and by the splitting of the TSSs at the DP induced by the out-of-plane component of magnetization even above the Curie temperature. The laser pump-probe experiment has shown that the difference in depopulation of the opposite branches of the DC states is practically not changed during the relaxation process. It allows to conclude that the SR-induced magnetization can be roughly estimated using the asymmetry in the intensity of the TSSs in PE spectra. Theoretical estimations have confirmed a possibility of the induced in-plane and out-of-plane magnetization by linearly polarized SR.

This finding should be taken into account in PE investigations of systems with helical spin structure, especially for magnetically-doped TIs, where the PE process can influence the spin structure in the ground state depending on photon energy and experimental details.

## Methods

The measurements of ARPES intensity maps for the DC states in pristine and magnetically-doped TIs presented in Fig. 1 and Supplementary Figs. 1S–3S were carried out at i3 beamline at MAXlab (Lund, Sweden) and BaDEIPh beamline at Elettra (Trieste, Italy) in the direction along the SR incidence plane (Geometry 1 in Fig. 8) and  $1^2$  end station at BESSY II (Helmholtz-Zentrum Berlin, Germany) in the direction perpendicular to the SR incidence plane (Geometry 2 in Fig. 8) using a Scienta R4000 or

SPECS Phoibos 150 analyzers. The incidence angle of SR for these experiments was  $73^\circ$  (MAXlab) and  $50^\circ$  (Elettra and BESSY II) relative to the surface normal.

The spin-resolved photoemission spectra for V-doped TIs were measured at the COPHEE setup at Swiss Light Source, Switzerland (Figs. 7(a,b)) and at the i3 beamline at MAXlab, Sweden (Supplementary Fig. 8S) with the spin orientation along the plane of the SR. The spin-resolved photoemission spectra were measured both for the in-plane and for the out-of-plane spin orientation. To increase the intensity of the TSSs in the region of the DP we used a photon energy range of 28-30 eV. For other photon energies the relative contribution of the DC states in the region of the DP is reduced. The SR incidence angle for these experiments was  $45^\circ$  and  $73^\circ$ .

The DC energy cut maps of the TSSs for  $\text{Bi}_{1.37}\text{V}_{0.03}\text{Sb}_{0.6}\text{Te}_2\text{Se}$  (Fig. 5 and Supplementary Fig. 6S) were measured at  $1^2$  station at BESSY II (Helmholtz-Zentrum Berlin, Germany) with a photon energy of 28 eV keeping the sample at the temperature of 55K and room temperature, respectively. The SR incidence angle was  $50^\circ$ .

The ARPES dispersion maps for magnetically-doped TIs, which were used for careful estimation of the splitting of the TSSs at the DP (Fig. 7) were measured at i3 beamline at MAXlab (Lund, Sweden), at the 9B beamline at HiSOR (Hiroshima, Japan) in the direction along the SR incidence plane (Geometry 1) and at  $1^3$  station at BESSY II (Helmholtz-Zentrum Berlin, Germany) in the direction perpendicular the plane of the SR incidence (Geometry 2). The SR incidence angle was  $45^\circ$  relative to the surface normal.

The time-resolved pump-probe laser experiment (Fig. 3) was carried out in ISSP at Tokyo University (Japan) for V-doped TI with stoichiometry  $\text{Bi}_{1.97}\text{V}_{0.03}\text{Te}_{2.4}\text{Se}_{0.6}$ . Time-resolved photoemission apparatus achieving sub-20-meV energy resolution and high stability was used, see details in Ref. [55]. The probe pulse was linearly  $p$ -polarized and with a photon energy of 5.9 eV. The pump pulse was  $s$ -polarized with  $h\nu=1.48$  eV. Geometry of the experiment is presented in Supplementary Fig. 4S. The laser beam incidence angle was  $45^\circ$  relative to the surface normal.

Part of work was carried out in the resource center “Physical methods of surface investigation” (PMSI) of Research park of Saint Petersburg State University.

The single crystals of pristine TIs  $\text{Bi}_{1.5}\text{Sb}_{0.5}\text{Te}_{1.8}\text{Se}_{1.2}$ ,  $\text{Bi}_2\text{Te}_2\text{Se}$  and  $\text{Bi}_{1.4}\text{Sb}_{0.6}\text{Te}_2\text{Se}$ , and magnetically-doped TIs  $\text{Bi}_{1.37}\text{V}_{0.03}\text{Sb}_{0.6}\text{Te}_2\text{Se}$ ,  $\text{Bi}_{1.3}\text{V}_{0.04}\text{Sb}_{0.66}\text{Te}_2\text{Se}$ , and  $\text{Bi}_{1.97}\text{V}_{0.03}\text{Te}_{2.4}\text{Se}_{0.6}$  were synthesized by using a modified vertical Bridgman method [56]. Clean surfaces of the TIs were obtained by a cleavage in ultrahigh vacuum. The base pressure during the experiments was better than  $1 \times 10^{-10}$  mbar.

## Acknowledgements

The authors acknowledge support by the Saint Petersburg State University (grant No. 15.61.202.2015), Russian Science Foundation grants No. 17-12-01333 (in the part of theoretical study of magnetic properties and ARPES analysis) and Russian Science Foundation grant No. 17-12-01047 (in part of crystal growth and the sample characterization). The work was also supported by the Spanish Ministry of Economy and Competitiveness MINECO (Project No. FIS2016-76617-P), German-Russian Interdisciplinary Science Center (G-RISC) funded by the German Federal Foreign Office via the German Academic Exchange Service (DAAD) and Russian-German laboratory at BESSY II (Helmholtz-Zentrum Berlin). The authors kindly acknowledge the MAXLab, HiSOR, SLS, Elettra, BESSY II, ISSP of the University of Tokyo and PMSI staff for technical support and help with experiment and useful discussions.

## Author contributions

The project was proposed by A.M.S., A.K.Z. The ARPES measurements were performed by I.I.K., D.M.S., V.Y.V., D.A.E., A.A.R., L.P., G.D.S., A.K., O.E.T., A.G.R. and A.M.S. The time-resolved ARPES measurements were performed by V.Y.V., A.K., Y.I., A.G.R. and A.M.S. Samples were synthesized and characterized by O.E.T., K.A.K. The experimental data analysis was carried out by A.M.S., A.A.R., D.M.S., V.Y.V., D.A.E. and I.I.K. Theoretical estimations and analysis of magnetic properties were performed by P.N.S., K.A.Z., A.K.Z. Calculations of PE spectra, ARPES dispersion maps and the TSS intensity asymmetry at different photon energies were performed and analysed by E.E.K., E.V.C. All authors extensively discussed the results and participated in the manuscript editing. The manuscript was written by A.M.S., E.E.K., P.N.S. and A.K.Z.

## Additional information

The authors declare that the data supporting the findings of this study are available within the paper and its supplementary information files. Supplementary information is available in the online version of the paper. Reprints and permissions information is available online at [www.nature.com/reprints](http://www.nature.com/reprints).

## Competing financial interests

The authors declare no competing financial interests.

## References

- [1] Hasan, M. Z. & Kane, C. L. Colloquium: Topological insulators. *Rev. Mod. Phys.* **82**, 3045–3067 (2010). URL <https://link.aps.org/doi/10.1103/RevModPhys.82.3045>.
- [2] Hsieh, D. *et al.* A tunable topological insulator in the spin helical Dirac transport regime. *Nature* **460**, 1101–1105 (2009). URL <http://dx.doi.org/10.1038/nature08234>.
- [3] Zhang, H. *et al.* Topological insulators in  $\text{Bi}_2\text{Se}_3$ ,  $\text{Bi}_2\text{Te}_3$  and  $\text{Sb}_2\text{Te}_3$  with a single Dirac cone on the surface. *Nat Phys* **5**, 438–442 (2009). URL <http://dx.doi.org/10.1038/nphys1270>.
- [4] Moore, J. Topological insulators: The next generation. *Nat Phys* **5**, 378–380 (2009). URL <http://dx.doi.org/10.1038/nphys1294>.
- [5] Hosur, P. Circular photogalvanic effect on topological insulator surfaces: Berry-curvature-dependent response. *Phys. Rev. B* **83**, 035309 (2011). URL <http://link.aps.org/doi/10.1103/PhysRevB.83.035309>.
- [6] Junck, A., Refael, G. & von Oppen, F. Photocurrent response of topological insulator surface states. *Phys. Rev. B* **88**, 075144 (2013). URL <http://link.aps.org/doi/10.1103/PhysRevB.88.075144>.
- [7] Mc Iver J., W., Hsieh, D., Steinberg, H., Jarillo-Herrero, P. & Gedik, N. Control over topological insulator photocurrents with light polarization. *Nat Nano* **7**, 96–100 (2012). URL <http://dx.doi.org/10.1038/nnano.2011.214>.
- [8] Ogawa, N. *et al.* Zero-bias photocurrent in ferromagnetic topological insulator. *Nature Communications* **7**, 12246 (2016).
- [9] Shikin, A. M. *et al.* Surface spin-polarized currents generated in topological insulators by circularly polarized synchrotron radiation and their photoelectron spectroscopy indication. *Physics of the Solid State* **58**, 1675–1686 (2016). URL <http://dx.doi.org/10.1134/S1063783416080266>.
- [10] Kastl, C., Karnetzky, C., Karl, H. & Holleitner, A. W. Ultrafast helicity control of surface currents in topological insulators with near-unity fidelity. *Nature Communications* **6**, 6617 (2015).
- [11] Li, C. H. *et al.* Electrical detection of charge-current-induced spin polarization due to spin-momentum locking in  $\text{Bi}_2\text{Se}_3$ . *Nat Nano* **9**, 218–224 (2014). URL <http://dx.doi.org/10.1038/nnano.2014.16>.
- [12] Mellnik, A. R. *et al.* Spin-transfer torque generated by a topological insulator. *Nature* **511**, 449–451 (2014). URL <http://dx.doi.org/10.1038/nature13534>.
- [13] Fan, Y. *et al.* Magnetization switching through giant spin-orbit torque in a magnetically doped topological insulator heterostructure. *Nat Mater* **13**, 699–704 (2014).
- [14] Shikin, A. M. *et al.* Out-of-plane polarization induced in magnetically-doped topological insulator  $\text{Bi}_{1.37}\text{V}_{0.03}\text{Sb}_{0.6}\text{Te}_2\text{Se}$  by circularly polarized synchrotron radiation above a Curie temperature. *Applied Physics Letters* **109**, 222404 (2016).
- [15] Qi, X.-L., Hughes, T. L. & Zhang, S.-C. Topological field theory of time-reversal invariant insulators. *Phys. Rev. B* **78**, 195424 (2008). URL <https://link.aps.org/doi/10.1103/PhysRevB.78.195424>.

- [16] Nomura, K. & Nagaosa, N. Surface-quantized anomalous Hall current and the magnetoelectric effect in magnetically disordered topological insulators. *Phys. Rev. Lett.* **106**, 166802 (2011). URL <https://link.aps.org/doi/10.1103/PhysRevLett.106.166802>.
- [17] Wang, J., Lian, B., Qi, X.-L. & Zhang, S.-C. Quantized topological magnetoelectric effect of the zero-plateau quantum anomalous Hall state. *Phys. Rev. B* **92**, 081107 (2015). URL <https://link.aps.org/doi/10.1103/PhysRevB.92.081107>.
- [18] Chang, C.-Z. *et al.* Experimental observation of the quantum anomalous Hall effect in a magnetic topological insulator. *Science* **340**, 167–170 (2013).
- [19] Chang, C.-Z. *et al.* High-precision realization of robust quantum anomalous Hall state in a hard ferromagnetic topological insulator. *Nat Mater* **14**, 473–477 (2015).
- [20] Yu, R. *et al.* Quantized anomalous Hall effect in magnetic topological insulators. *Science* **329**, 61 (2010). URL <http://science.sciencemag.org/content/329/5987/61.abstract>.
- [21] Neupane, M. *et al.* Gigantic surface lifetime of an intrinsic topological insulator. *Phys. Rev. Lett.* **115**, 116801 (2015). URL <https://link.aps.org/doi/10.1103/PhysRevLett.115.116801>.
- [22] Crepaldi, A. *et al.* Evidence of reduced surface electron-phonon scattering in the conduction band of Bi<sub>2</sub>Se<sub>3</sub> by nonequilibrium ARPES. *Phys. Rev. B* **88**, 121404 (2013). URL <https://link.aps.org/doi/10.1103/PhysRevB.88.121404>.
- [23] Hajlaoui, M. *et al.* Tuning a Schottky barrier in a photoexcited topological insulator with transient Dirac cone electron-hole asymmetry. *Nature Communications* **5**, 3003 (2014).
- [24] Ishida, Y. *et al.* Emergent photovoltage on SmB<sub>6</sub> surface upon bulk-gap evolution revealed by pump-and-probe photoemission spectroscopy. *Scientific Reports* **5**, 8160 (2015).
- [25] Chernyshov, A. *et al.* Evidence for reversible control of magnetization in a ferromagnetic material by means of spin-orbit magnetic field. *Nat Phys* **5**, 656–659 (2009).
- [26] Zhang, H., Liu, C.-X. & Zhang, S.-C. Spin-orbital texture in topological insulators. *Phys. Rev. Lett.* **111**, 066801 (2013). URL <https://link.aps.org/doi/10.1103/PhysRevLett.111.066801>.
- [27] Cao, Y. *et al.* Mapping the orbital wavefunction of the surface states in three-dimensional topological insulators. *Nat Phys* **9**, 499–504 (2013).
- [28] Zhu, Z.-H. *et al.* Layer-by-layer entangled spin-orbital texture of the topological surface state in Bi<sub>2</sub>Se<sub>3</sub>. *Phys. Rev. Lett.* **110**, 216401 (2013). URL <http://link.aps.org/doi/10.1103/PhysRevLett.110.216401>.
- [29] Zhu, Z.-H. *et al.* Photoelectron spin-polarization control in the topological insulator Bi<sub>2</sub>Se<sub>3</sub>. *Phys. Rev. Lett.* **112**, 076802 (2014). URL <http://link.aps.org/doi/10.1103/PhysRevLett.112.076802>.
- [30] Seibel, C. *et al.* Photoelectron spin polarization in the Bi<sub>2</sub>Te<sub>3</sub>(0001) topological insulator: Initial- and final-state effects in the photoemission process. *Phys. Rev. B* **93**, 245150 (2016). URL <https://link.aps.org/doi/10.1103/PhysRevB.93.245150>.
- [31] Jozwiak, C. *et al.* Photoelectron spin-flipping and texture manipulation in a topological insulator. *Nat Phys* **9**, 293–298 (2013). URL <http://dx.doi.org/10.1038/nphys2572>.
- [32] Park, C.-H. & Louie, S. G. Spin polarization of photoelectrons from topological insulators. *Phys. Rev. Lett.* **109**, 097601 (2012). URL <http://link.aps.org/doi/10.1103/PhysRevLett.109.097601>.
- [33] Jozwiak, C. *et al.* Widespread spin polarization effects in photoemission from topological insulators. *Phys. Rev. B* **84**, 165113 (2011). URL <http://link.aps.org/doi/10.1103/PhysRevB.84.165113>.
- [34] Neupane, M. *et al.* Oscillatory surface dichroism of the insulating topological insulator Bi<sub>2</sub>Te<sub>2</sub>Se. *Phys. Rev. B* **88**, 165129 (2013). URL <http://link.aps.org/doi/10.1103/PhysRevB.88.165129>.
- [35] Xu, S.-Y. *et al.* Hedgehog spin texture and Berry’s phase tuning in a magnetic topological insulator. *Nat Phys* **8**, 616–622 (2012). URL <http://dx.doi.org/10.1038/nphys2351>.

- [36] Miyamoto, K. *et al.* Topological surface states with persistent high spin polarization across the Dirac point in  $\text{Bi}_2\text{Te}_2\text{Se}$  and  $\text{Bi}_2\text{Se}_2\text{Te}$ . *Phys. Rev. Lett.* **109**, 166802 (2012). URL <http://link.aps.org/doi/10.1103/PhysRevLett.109.166802>.
- [37] Shikin, A. M. *et al.* Electronic and spin structure of the topological insulator  $\text{Bi}_2\text{Te}_{2.4}\text{Se}_{0.6}$ . *Phys. Rev. B* **89**, 125416 (2014). URL <http://link.aps.org/doi/10.1103/PhysRevB.89.125416>.
- [38] Tang, C. S. *et al.* Terahertz conductivity of topological surface states in  $\text{Bi}_{1.5}\text{Sb}_{0.5}\text{Te}_{1.8}\text{Se}_{1.2}$ . *Scientific Reports* **3**, 3513 (2013). URL <http://dx.doi.org/10.1038/srep03513>.
- [39] Adawi, I. Theory of the surface photoelectric effect for one and two photons. *Phys. Rev.* **134**, A788–A798 (1964).
- [40] Krasovskii, E. E. & Schattke, W. Calculation of the wave functions for semi-infinite crystals with linear methods of band theory. *Phys. Rev. B* **59**, R15609–R15612 (1999).
- [41] Krasovskii, E. E., Starrost, F. & Schattke, W. Augmented fourier components method for constructing the crystal potential in self-consistent band-structure calculations. *Phys. Rev. B* **59**, 10504–10511 (1999).
- [42] Koelling, D. D. & Harmon, B. N. A technique for relativistic spin-polarised calculations. *J. Phys. C* **10**, 3107 (1977).
- [43] DiSalvo, F. J. Thermoelectric cooling and power generation. *Science* **285**, 703–706 (1999). URL <http://science.sciencemag.org/content/285/5428/703>. <http://science.sciencemag.org/content/285/5428/703.full.pdf>.
- [44] Xia, Y. *et al.* Observation of a large-gap topological-insulator class with a single dirac cone on the surface. *Nature Physics* **5**, 398–402 (2009).
- [45] Sirotnin, Y. I. & Shaskolskaya, M. P. *Basic crystallophysics* (Moscow: Science, 1979).
- [46] Meier, F. & Zakharchenya, B. P. (eds.) *Optical orientation* (Elsevier, 2012).
- [47] Rosenberg, G. & Franz, M. Surface magnetic ordering in topological insulators with bulk magnetic dopants. *Phys. Rev. B* **85**, 195119 (2012).
- [48] Liu, Q., Liu, C.-X., Xu, C., Qi, X.-L. & Zhang, S.-C. Magnetic impurities on the surface of a topological insulator. *Phys. Rev. Lett.* **102**, 156603 (2009).
- [49] Zhu, J.-J., Yao, D.-X., Zhang, S.-C. & Chang, K. Electrically controllable surface magnetism on the surface of topological insulators. *Phys. Rev. Lett.* **106**, 097201 (2011).
- [50] Henk, J. *et al.* Topological character and magnetism of the Dirac state in Mn-doped  $\text{Bi}_2\text{Te}_3$ . *Phys. Rev. Lett.* **109**, 076801 (2012). URL <https://link.aps.org/doi/10.1103/PhysRevLett.109.076801>.
- [51] Semenov, Y. G., Li, X. & Kim, K. W. Tunable photogalvanic effect on topological insulator surfaces via proximity interactions. *Phys. Rev. B* **86**, 201401 (2012). URL <https://link.aps.org/doi/10.1103/PhysRevB.86.201401>.
- [52] Shikin, A. M. *et al.* Anomalously large gap and induced out-of-plane spin polarization in magnetically doped 2D Rashba system: V-doped  $\text{BiTeI}$ . *2D Materials* **4**, 025055 (2017). URL <http://stacks.iop.org/2053-1583/4/i=2/a=025055>.
- [53] Schmidt, T. M., Miwa, R. H. & Fazzio, A. Spin texture and magnetic anisotropy of Co impurities in  $\text{Bi}_2\text{Se}_3$  topological insulators. *Phys. Rev. B* **84**, 245418 (2011).
- [54] Vergniory, M. G. *et al.* Exchange interaction and its tuning in magnetic binary chalcogenides. *Phys. Rev. B* **89**, 165202 (2014). URL <http://link.aps.org/doi/10.1103/PhysRevB.89.165202>.
- [55] Ishida, Y. *et al.* Time-resolved photoemission apparatus achieving sub-20-meV energy resolution and high stability. *Review of Scientific Instruments* **85**, 123904 (2014).
- [56] Kokh, K. A., Makarenko, S. V., Golyashov, V. A., Shegai, O. A. & Tereshchenko, O. E. Melt growth of bulk  $\text{Bi}_2\text{Te}_3$  crystals with a natural p-n junction. *CrystEngComm* **16**, 581–584 (2014). URL <http://dx.doi.org/10.1039/C3CE42026D>.

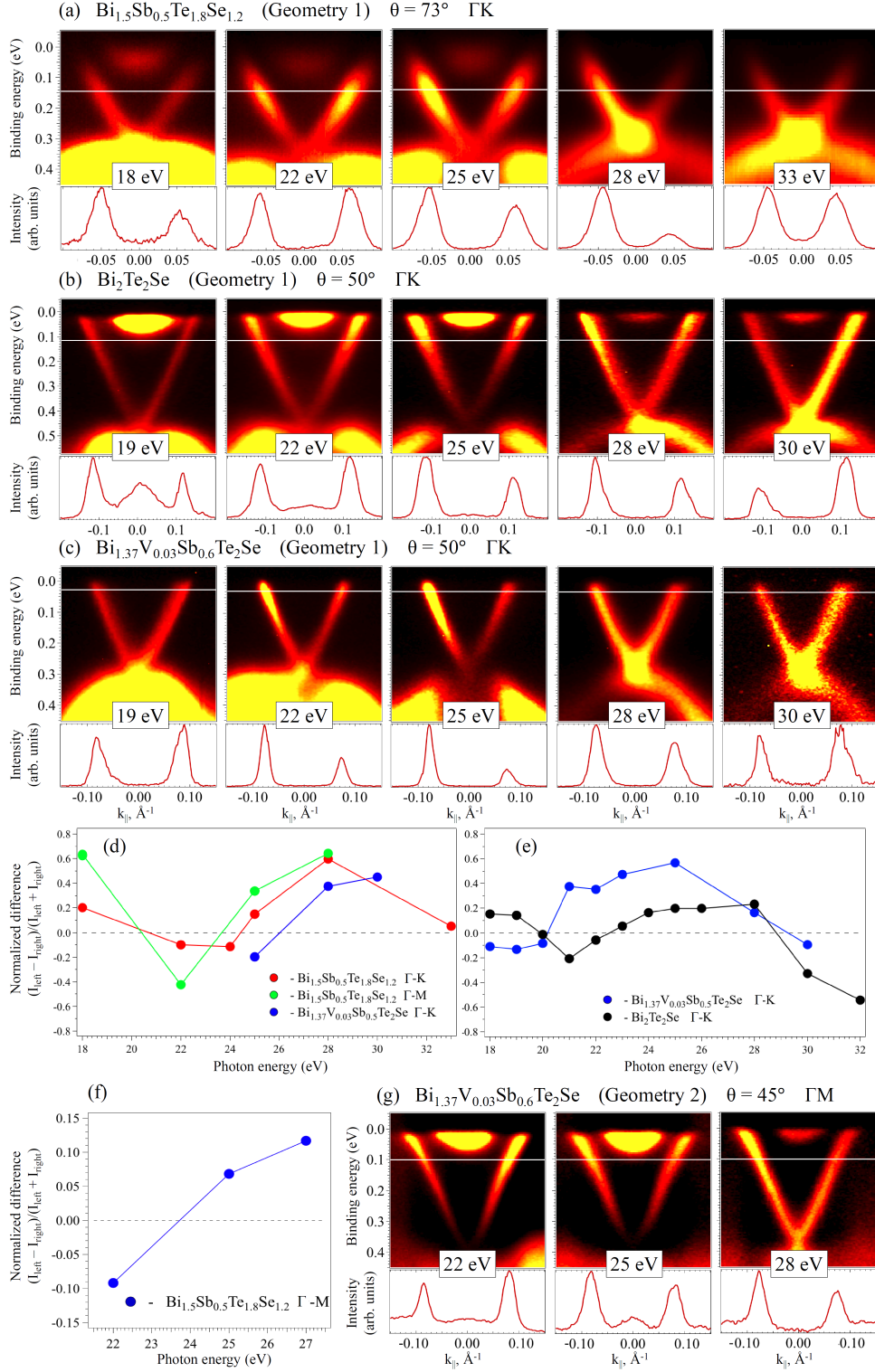


**Figure 1:** Lines (a,b,c) – series of ARPES intensity maps of the TSSs measured along the SR incidence plane ( $\Gamma\text{K}$ ) (Geometry 1) for pristine TIs with stoichiometry  $\text{Bi}_{1.5}\text{Sb}_{0.5}\text{Te}_{1.8}\text{Se}_{1.2}$ ,  $\text{Bi}_2\text{Te}_2\text{Se}$  and for V-doped TIs with stoichiometry  $\text{Bi}_{1.37}\text{V}_{0.03}\text{Sb}_{0.6}\text{Te}_2\text{Se}$ , accordingly, by using linear  $p$ -polarized SR at different photon energy. The profiles of comparable intensities of the TSSs with opposite momenta cut at the energy corresponding to enhanced intensity (marked by horizontal white lines) are presented at the bottom of each insets. (d,e) – The TSS intensity asymmetry ( $A$ ) trend vs photon energy estimated from the ARPES intensity maps presented in lines (a,b,c) and Supplementary Figs. 1S, 2S measured along  $\Gamma\text{K}$  and  $\Gamma\text{M}$  directions of the Brillouin zone. (g) – Similar ARPES intensity maps measured in the direction perpendicular to the SR incidence plane (Geometry 2) for pristine TIs with stoichiometry  $\text{Bi}_{1.5}\text{Sb}_{0.5}\text{Te}_{1.8}\text{Se}_{1.2}$  and (f) – corresponding variation of the TSS intensity asymmetry ( $A$ ).



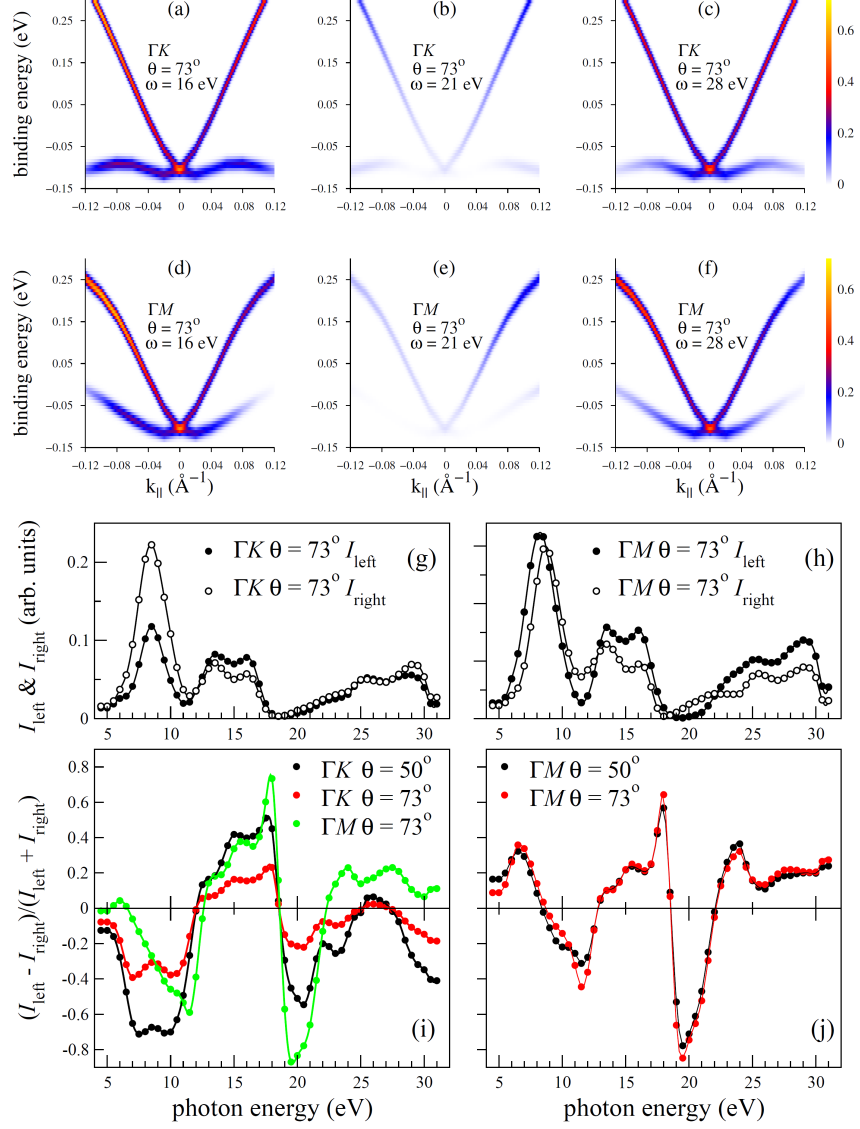


**Figure 2:** (a-f) Calculated energy-momentum distribution of the photoemission intensity from the DC surface states along  $\bar{\Gamma}\bar{K}$  (a-c) and along  $\bar{\Gamma}\bar{M}$  (d-f) for the three photon energies:  $\hbar\nu = 16$  (a,d), 21 (b,e), and 18 eV (c,f). In all cases a  $p$ -polarized light is incident along  $\bar{\Gamma}\bar{K}$  at an angle of  $\theta = 73^\circ$ . (g,h) Photon energy dependence of the total intensity from the upper Dirac cone integrated over negative  $k_{\parallel}$  ( $I_{\text{left}}$ , full circles) and positive  $k_{\parallel}$  ( $I_{\text{right}}$ , open circles) for  $k_{\parallel}$  along  $\bar{\Gamma}\bar{K}$  (g) and along  $\bar{\Gamma}\bar{M}$  (h). (i,j) Normalized difference between the integrated intensities in the opposite directions,  $[I_{\text{left}}(\hbar\nu) - I_{\text{right}}(\hbar\nu)]/[I_{\text{left}}(\hbar\nu) + I_{\text{right}}(\hbar\nu)]$  for two angles of incidence,  $\theta = 50$  and  $73^\circ$ . In graph (i) the light incidence plane is parallel to  $\mathbf{k}_{\parallel}$  (both for  $\bar{\Gamma}\bar{K}$  and for  $\bar{\Gamma}\bar{M}$ ), and in graph (j) it is perpendicular to  $\mathbf{k}_{\parallel}$  ( $\bar{\Gamma}\bar{M}$ ).

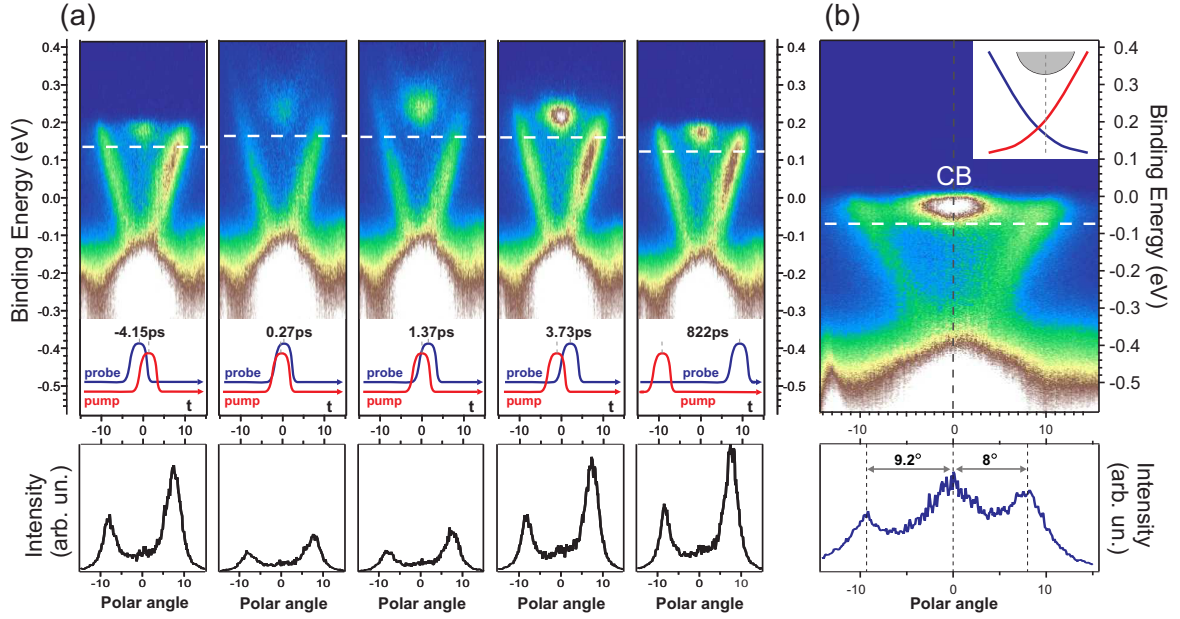


**Figure 3:** (a) – Time-resolved ARPES maps measured by laser pump-probe experiment for  $\text{Bi}_{1.97}\text{V}_{0.03}\text{Te}_{2.4}\text{Se}_{0.6}$  at 11 K by using  $p$ -polarized probe pulse ( $h\nu=5.9$  eV) and  $s$ -polarized pump pulse ( $h\nu=1.48$  eV). The delay time between pump and probe pulses is shown below the ARPES maps. In the bottom line the time-resolved TSS intensity profiles cut at the energy close to the CB states is shown. (b) –  $k_{\parallel}$ -shift of the ARPES dispersion map measured by using  $p$ -polarized probe pulse relative to the CB states located at the Fermi level at  $k_{\parallel} = 0$ . Schematic presentation of the  $k_{\parallel}$ -shift is shown in inset. Below the ARPES map the corresponding profile of the intensities of the TSSs and CB states confirming the  $k_{\parallel}$ -shift of the DC states due to induced in-plane magnetic field is shown.

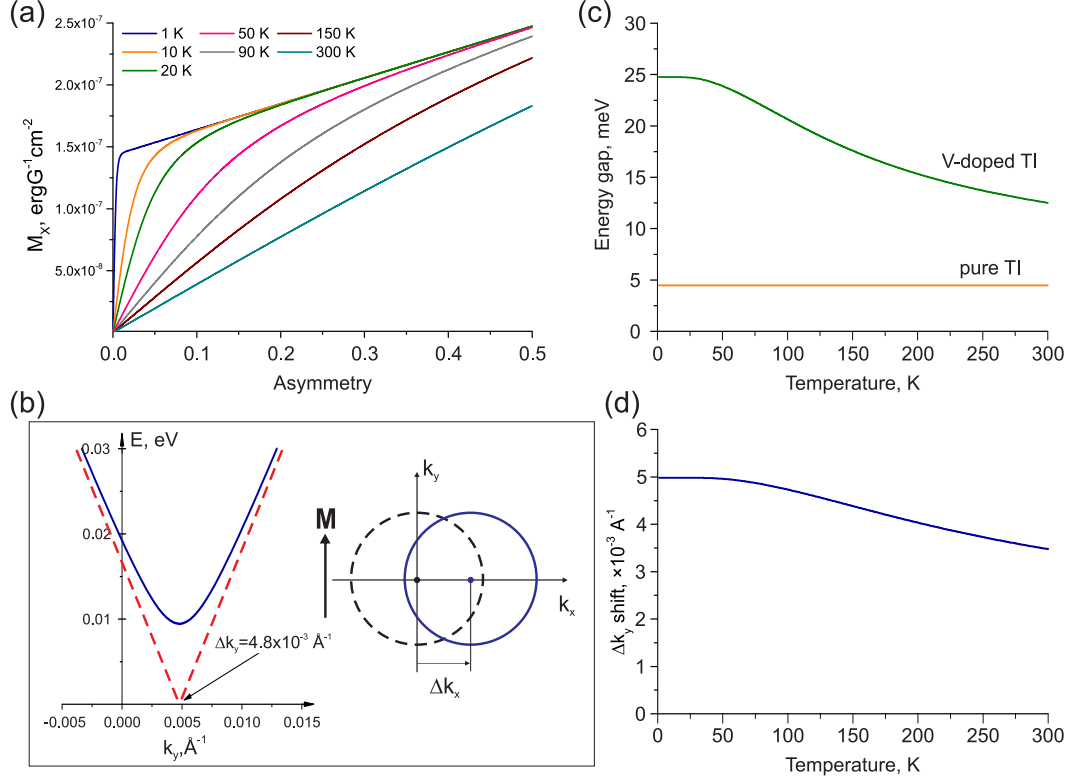
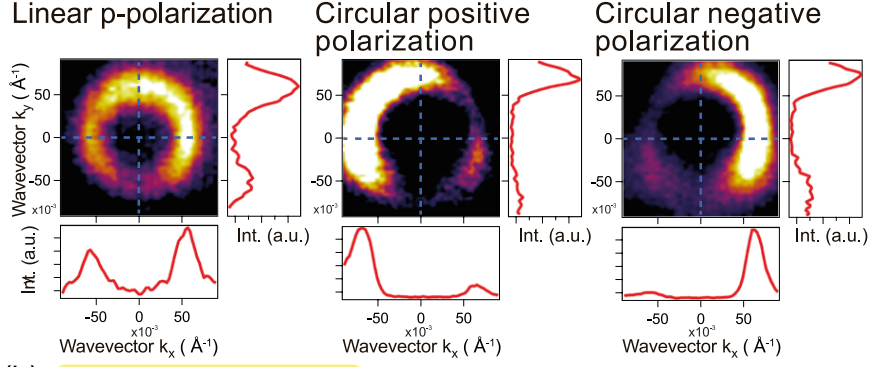
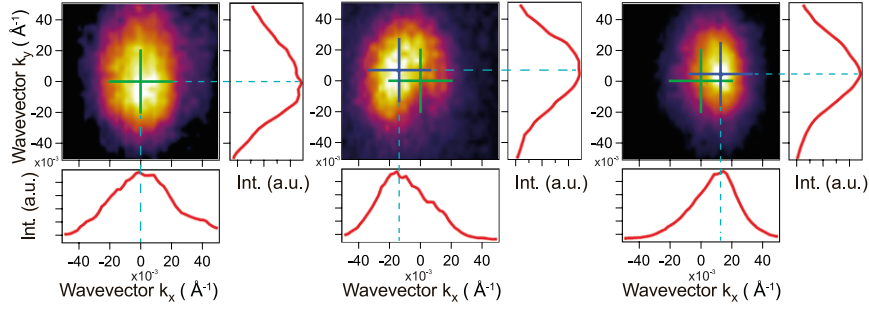


**Figure 4:** (a) – Calculated dependence of the in-plane component of a total SR-induced magnetization vs the asymmetry in the hole-generation with opposite spins (A) for different temperatures between 1 and 300 K. (b) – Modification of the DC state dispersions obtained at crossing by the plane ( $k_x=0$ ) which indicate the influence of the out-of-plane and in-plane components of induced magnetization (opening the gap at the DP and the  $k_x$ -shift of the DC states). (c,d) – Calculated temperature dependences of the energy gap at the DP due to the out-of-plane component of the induced magnetization for magnetically-doped and pristine TIs and corresponding  $k_{\parallel}$ -shift of the DP relative to  $k_{\parallel} = 0$  in the direction orthogonal to the magnetization as a function of temperature.

(a) Dirac point energy cuts



(b) Dirac point position



(c) Influence of induced magnetization

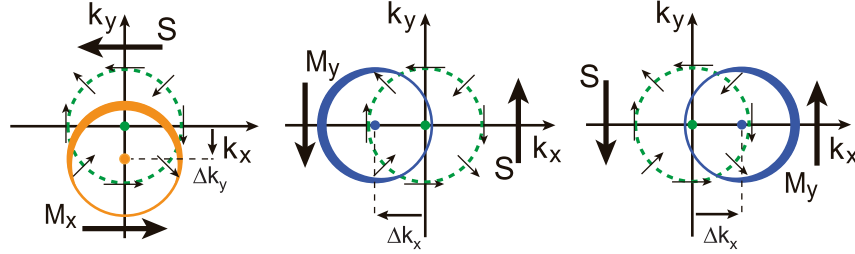


**Figure 5:** The  $(k_x, k_y)$ -projections of the DC state maps cut at the energy near the Fermi level – (a) and at the DP – (b) measured at 55 K for  $\text{Bi}_{1.37}\text{V}_{0.03}\text{Sb}_{0.6}\text{Te}_2\text{Se}$  with different polarization of SR. Below and on the right side of the maps the corresponding profiles of the TSS intensity showing the distribution of the TSS intensity along  $k_x$  and  $k_y$  are presented. A pronounced asymmetry in the TSS intensity which is a source for the corresponding uncompensated spin accumulation is visible for different polarization of SR. Line (b) shows the  $(k_x, k_y)$ -shift of the DP positions using linearly  $p$ -polarized SR (marked by green crosses) and opposite circularly-polarized SR (blue crosses) under induced in-plane magnetization generated by SR. Line (c) – schematic presentations of the relation of the asymmetry in the TSS intensity, the directions of the induced uncompensated spin accumulation ( $S$ ) and the in-plane magnetization ( $M$ ) and the directions of the  $(k_x, k_y)$ -shift of the DC position due to induced magnetization.

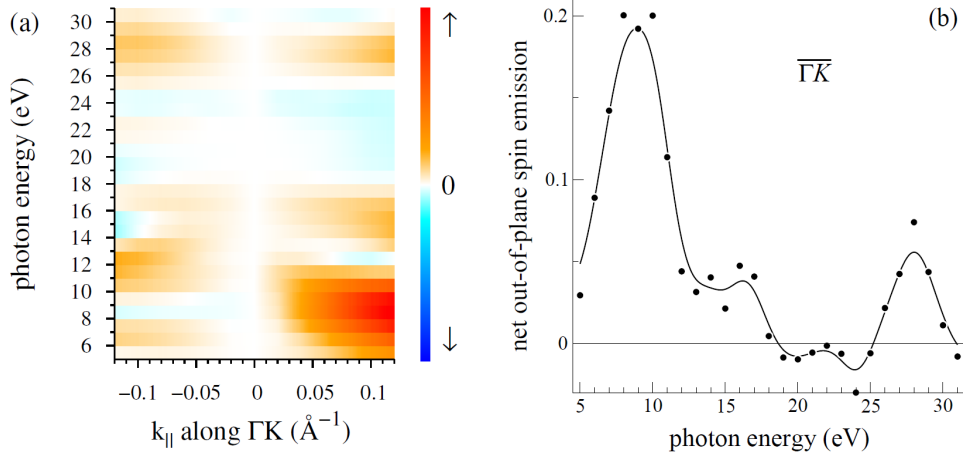


**Figure 6:** (a) Calculated photon-energy dependence of the  $k_{\parallel}$ -distribution  $S(k_{\parallel}, h\nu)$  of the net out-of-plane spin in photoelectrons excited by a  $p$ -polarized SR along the SR incidence plane ( $\Gamma\bar{K}$ ) from the upper DC of  $\text{Bi}_2\text{Te}_2\text{Se}$  for  $h\nu$  from 5 to 31 eV. (b) Photon energy dependence of the net out-of-plane spin integrated over  $k_{\parallel}$  from  $-0.12$  to  $0.12 \text{ \AA}^{-1}$  along  $\Gamma\bar{K}$ .

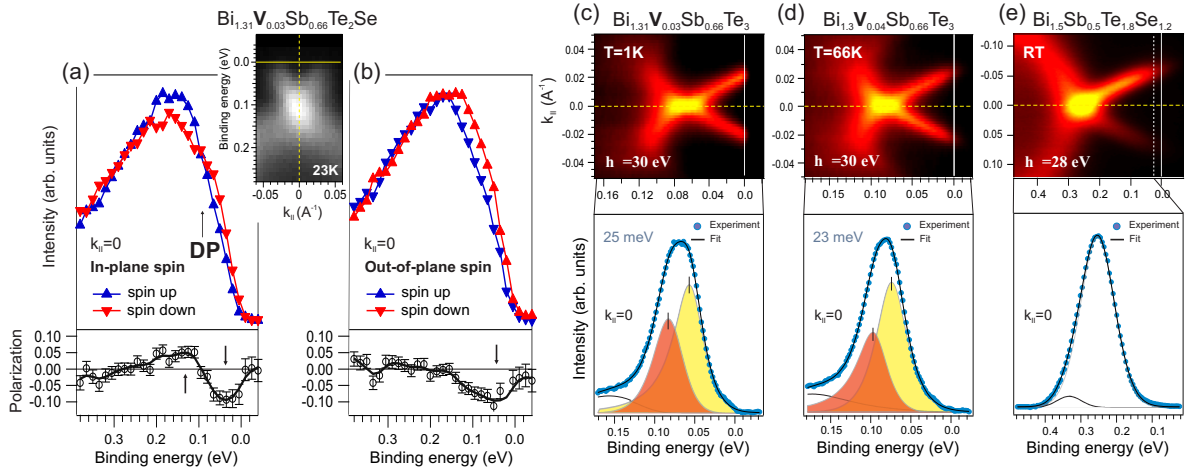


**Figure 7:** (a,b) – In-plane and out-of-plane spin-resolved PE spectra measured at the DP for  $\text{Bi}_{1.31}\text{V}_{0.03}\text{Sb}_{0.66}\text{Te}_2\text{Se}$  at a temperature of 23 K and a photon energy  $h\nu = 30 \text{ eV}$  using linear  $p$ -polarized SR. Corresponding experimental asymmetries for opposite spin polarization including the experimental uncertainty for each point of the measurements are shown below the spin-resolved spectra. (c-e): Upper – ARPES intensity maps measured for V-doped – (c,d) and pristine – (e) TIs at different temperatures and photon energies 28 and 30 eV. Bottom – corresponding spectra measured at the DP and the result of the fitting procedure with decomposition on spectral components.

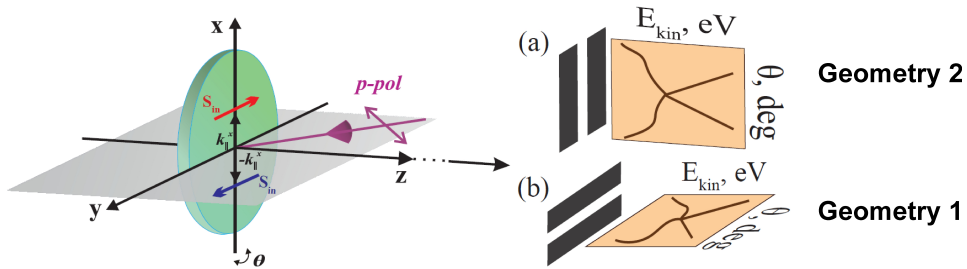


**Figure 1M 8: METHODS Section.** Schematic presentation of the ARPES measurement geometries with the analyzer slit oriented along (Geometry 1) and perpendicular (Geometry 2) to the of SR incidence plane.